Int. J. Heat Mass Transfer. Vol. 29, No. 11, pp. 1639–1648, 1986
Printed in Great Britain

0017-9310/86 $3.00 + 0.00
Pergamon Journals Ltd.

Prediction of the critical heat flux in flow boiling at intermediate qualities

S. H. YING and J. WEISMAN

Department of Chemical and Nuclear Engineering, University of Cincinnati, Cincinnati, OH 45221-0171, U.S.A.

(*Received* 27 *August* 1985 *and in final form* 28 *January* 1986)

Abstract—By allowing for a non-uniform void profile, it is found that the previously developed, theoretically based critical heat flux (CHF) prediction procedure can be extended to void fractions of up to 0.8. The general approach holds for both round tubes and rod bundles with simple spacers. Both water and non-water data are predicted by this approach. The ability to predict CHF at higher qualities allowed the predictive procedure to be extended to lower mass flow rates where the void fractions at CHF are generally high.

THE CRITICAL heat flux is an important limitation which must be avoided in the design of boiling heat transfer systems. Although theoretically based predictions of the critical heat flux (CHF) in pool boiling [1] and in flow boiling at high qualities [2, 3] have been available for some time, successful theoretically based CHF predictions for flow boiling at subcooled and low quality conditions are relatively recent.

It is now generally recognized that the mechanism governing low quality and subcooled CHF differs substantially from that governing CHF at high vapor qualities. To distinguish between the two mechanisms, low quality CHF is often referred to as "departure from nucleate boiling" (DNB). The phenomenologically derived DNB prediction procedure of Weisman and Pei [4] is based on the existence of a bubbly layer adjacent to the heated wall [5, 6]. The critical heat flux is assumed to occur when the bubbles in this layer become so crowded that they agglomerate into a continuous film. It is further assumed that the rate of liquid transport to the bubbly layer, as determined by the turbulent interchange at the outer edge of the bubbly layer, is the limiting mechanism. By using a simple mass balance over the bubbly layer, it is found that:

$$q''_{DNB}/(h_{fg}G') = (x_2 - x_1)\left(\frac{h_f - h_{id}}{h_i - h_{id}}\right). \quad (1)$$

The value of x was calculated, using the homogeneous flow assumption, as that quality which corresponds to the maximum void fraction which is possible in a layer of independent bubbles. This void fraction was estimated to be 0.82 for elliptical bubbles. The value of x_1 is obtained from a heat balance with proper allowance for thermodynamic non-equilibrium.

The quantity G' represents the mass flow rate due to turbulent interchange at the edge of the bubbly layer. This flow is determined by:

$$G' = \psi i_b G. \quad (2)$$

The parameter i_b, representing the turbulent intensity at the bubbly layer–core interface, is calculated as the product of the single-phase turbulent intensity at the bubbly layer edge and a two-phase enhancement factor. The resulting expression is:

$$i_b = 0.462(k)^{0.6}(Re)^{-0.1}(D_p/d)^{0.6}(1 + a(\rho_L - \rho_G)/\rho_G), \quad (3)$$

where

$$a = 0.135 \quad G \leqslant 9.7 \times 10^6\ \text{kg/h m}^2$$

$$a = 0.135(G/9.7 \times 10^6)^{-0.3} \quad G > 9.7 \times 10^6\ \text{kg/h m}^2.$$

Through consideration of the velocity fluctuations that are effective in reaching the wall, the parameter ψ was computed to be:

$$\psi = \frac{1}{\sqrt{2\pi}} \exp\left[-1/2\left(\frac{v_{11}}{\sigma_{v'}}\right)^2\right] - 1/2\left(\frac{v_{11}}{\sigma_{v'}}\right) \operatorname{erfc}\left(\frac{v_{11}}{\sqrt{2}\sigma_{v'}}\right), \quad (4)$$

Calculation details are provided by Weisman and Pei [4] in the appendix to their paper.†

The original work showed that this procedure predicted DNB heat fluxes in water, refrigerants, anhydrous ammonia, and liquid nitrogen with good accuracy. Weisman and Ying [7] subsequently extended the work to lower mass velocities and to rod bundles [8, 9]. With the lower velocity extension, the Weisman–Pei predictive procedure applies over the

† In the Appendix to the Weisman–Pei paper, there is a typographical error in the equation for y_b^+. This equation should read: $y_b^+ = 0.01(\sigma g_c D_p \rho_L)^{1/2}/(\mu_L)$.

NOMENCLATURE

a	two-phase multiplier in turbulent intensity equation
C_1, C_2, C_B, C_F, C_S	constants
d	tube diameter (length)
D_h	hydraulic diameter (length)
D_p	average bubble diameter (length)
f	friction factor
G	total axial mass velocity [mass/(length^2 time)]
G'	lateral mass velocity from core to bubbly layer due to turbulence [mass/(length^2 time)]
g	gravitational acceleration (length/time^2)
g_c	gravitational conversion factor [(mass-length)/(force)(time)^2)]
h_f	saturated liquid enthalpy (energy/mass)
h_{fg}	evaporation enthalpy change (energy/mass)
h_l	enthalpy of liquid (energy/mass)
h_{ld}	enthalpy at point of bubble detachment (energy/mass)
i_b	turbulent intensity at bubbly layer–core interface
k	constant
K, K'	constants
L	tube length
q''_{DNB}	DNB heat flux [energy/(length^2 time)]
r	radial position (length)
r_b	radius of bubble (length)
r_o	outer radius of tube (length)
R	(predicted CHF)/(measured CHF)
Re	Reynolds number
u_t	bubble rise velocity (length/time)
v_{11}	radial velocity created by vapor generation [length/time]
v'	radial fluctuating velocity [length/time]
$\bar{v}'$	mean values of v'
x_1	average quality in core region
x_{eff}	quality corresponding to α_{eff}
x_2	average quality in bubbly layer
z_{CHF}	axial distance at which CHF occurs (length).

Greek symbols

$\bar{\alpha}$	average void fraction in core
α	void fraction
α_{eff}	void fraction in core at edge of bubbly layer
α_{CHF}	void fraction of bubbly layer at CHF
β_0	contact angle (deg)
ψ	$\left\{\frac{1}{2\pi}\exp-\left[-\frac{1}{2}\left(\frac{v_{11}}{\sigma_{v'}}\right)^2\right] - \frac{1}{2}\left(\frac{v_{11}}{\sigma_{v'}}\right)\mathrm{erfc}\left(\frac{1}{\sqrt{2}}\frac{v_{11}}{\sigma_{v'}}\right)\right\}$
ρ_L	liquid density at bulk temperature (mass/length^3)
ρ_f	density of saturated liquid (mass/length^3)
ρ_G	vapor density (mass/length^3)
$\bar{\rho}$	average density (across entire flow area) [mass/length^3]
σ	surface tension [force/length]
$\sigma_{v'}$	standard deviation of v'
$\sigma(R)$	standard deviation of R
τ_ω	shear stress at wall [force/length^2]
μ_{avg}	viscosity of mixture [mass/(length time)]
μ_l	viscosity of liquid [mass/(length time)]
$\mu(R)$	mean value of R.

following range:

$$0.012 \leqslant \rho_G/\rho_L \leqslant 0.41$$

$$1.8 \times 10^6\,\mathrm{kg/m^2\,h} \leqslant G \leqslant 49 \times 10^6\,\mathrm{kg/m^2\,h}$$

$$0.35\,\mathrm{cm} \leqslant L \leqslant 360\,\mathrm{cm}$$

$$0.115\,\mathrm{cm} \leqslant d \leqslant 3.75\,\mathrm{cm}$$

$$\alpha_{CHF} \leqslant 0.6.$$

It will be observed that the requirement that $\alpha_{CHF} \leqslant 0.6$ poses a significant limitation at lower pressures. Thus for water and steam at 140 bar, the CHF quality cannot exceed 18% while at 35 bar it is limited to only about 3%. The present note therefore examines how the Weisman–Pei approach may be extended to higher void fractions.

EXAMINATION OF ROUND TUBE BEHAVIOR AT $\alpha > 0.6$

The round tube water data compiled by Thompson and Macbeth [10] were used to determine the effect of void fraction on Weisman–Pei predictions for core void fractions in excess of 0.6. To be consistent with the previous extension to low mass velocities [7], void fractions are related to quality by assuming that the bubble velocity is equal to the liquid velocity plus a bubble rise velocity, u_t, given by

$$u_t = 1.53[(\rho_L - \rho_G)\sigma g g_c/\rho_L^2]^{1/4}. \quad (5)$$

In the bubbly layer, the average liquid velocity is taken as one half of the velocity at the bubbly layer edge.

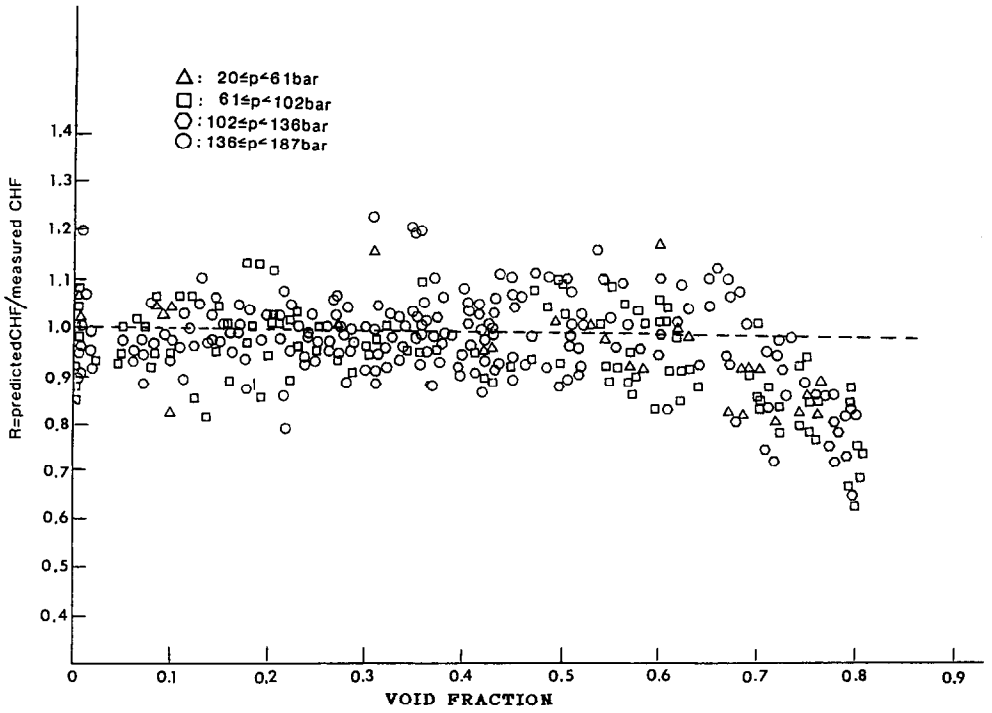

FIG. 1. Effect of void fraction on CHF predictions.

(See Ref. 8 for justification and full calculational procedure.)

The results of the critical heat flux predictions were expressed in terms of the ratio R where

$$R = \frac{\text{predicted DNB flux}}{\text{measured DNB flux}}. \quad (6)$$

The results are shown in Fig. 1 where R is plotted vs α. All of the water data for $0.6 < \alpha \leqslant 0.9$ are shown. However, due to the very large number of low void data points (1500) only a portion (20%) of these are shown.

As may be seen from Fig. 1. the predictive procedure works well up to void fraction of about 0.64. At higher void fractions the predictions are too low. However, no significant increase in data scatter is seen thus indicating that the basic correlating procedure still has validity.

EXPLANATION OF PREDICTION BEHAVIOR AT $\alpha > 0.64$

The average void fraction at which deviations from CHF predictions are first observed is well below that at which dry-out is to be expected. The explanation for the behavior seen therefore does not lie in a change in the CHF mechanism but rather in the violation of one of the assumptions made originally for low void fractures.

At low void fractions, the assumption of an essentially flat void profile across the central core is appropriate. Hence, assuming that the bubbly layer exchanges with fluid at the average quality is reasonable at low void fractions. However, as the average void fraction increases this is no longer true. The void profile is no longer flat and the fluid interchanging with the bubbly layer is at a void fraction which is below the average.

Based on the low pressure air–water observation of Serizawa [11] as reported on by Drew and Lahey [12], and the more recent data of Van der Welle [13], the void profile in the central fluid core begins to assume a parabolic shape as the average void fraction increases. This is illustrated in Fig. 2 which shows the height of

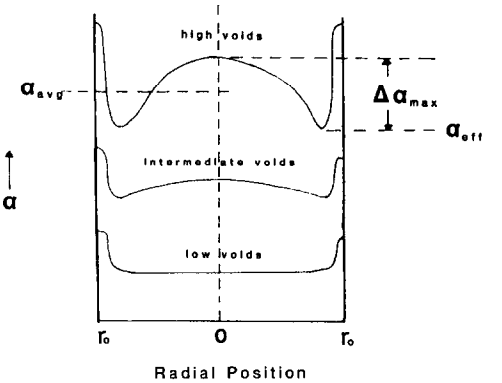

FIG. 2. Void fraction profiles.

the parabola to increase as the average void fraction increases. The Van der Welle [13] and Serizawa data [11, 12] indicate significant deviations from a flat void profile in the vicinity of $\bar{\alpha} \simeq 0.2$. This is near where the transition from bubbly to intermittent (plug or churn) flow is likely to occur for the [14] air–water system. The correlation of McQuillan and Whalley [14] indicates that, for high pressure steam under adiabatic conditions, the transition is in the neighborhood of $\alpha \simeq 0.5$. One would not expect significant deviation from a flat void profile until outside of the bubbly region which, for the high pressure systems of interest, means void fractions in excess of 50%. Further, the high vaporization rates in DNB test sections probably lead to flatter void profiles than in the adiabatic case. Hence, corrections for the effect of void fraction profile which begin at void fractions of the order of 0.6 are not unreasonable.

The parabolic void fraction profile of Fig. 2 may be represented by

$$\alpha = \alpha_{\text{eff}} + \Delta\alpha_{\max}[1-(r/r_0)^2] \tag{7}$$

where

$\Delta\alpha_{\max}$ = value of α at tube centerline—α_{eff}.

For such a distribution

$$\bar{\alpha} - \alpha_{\text{eff}} = \frac{\Delta\alpha_{\max}}{2} \tag{8}$$

or

$$\alpha_{\text{eff}} = \bar{\alpha} - \frac{\Delta\alpha_{\max}}{2}. \tag{9}$$

From Serizawa's data, it is concluded that $\Delta\alpha_{\max}$ increases as $\bar{\alpha}$ increases. If a linear relationship is assumed, we have,

$$\Delta\alpha_{\max} = K[\bar{\alpha} - \alpha_0], \tag{10}$$

where α_0 = average void fraction below which the void profile may be taken as flat.

Then

$$\alpha_{\text{eff}} = \alpha_{\text{avg}} - K(\bar{\alpha} - \alpha_0). \tag{11}$$

Since the bubbly layer exchanges fluid with the core fluid at its edge, the interchange is with fluid having a void fraction α_{eff}. We therefore define $(x_1)_{\text{eff}}$ such that

$$(x_1)_{\text{eff}} = \text{quality corresponding to } \alpha_{\text{eff}} \tag{12}$$

and then rewrite equation (1) as

$$q''_{\text{DNB}}/(h_{\text{fg}}G') = (x_2 - x_{1_{\text{eff}}})\left(\frac{h_{\text{f}} - h_{\text{id}}}{h_{\text{l}} - h_{\text{id}}}\right). \tag{13}$$

The experimental data is then used to determine an appropriate value for K in equation (11).

CORRELATION OF EXPERIMENTAL DATA

It was found that the underprediction of the round tube data shown in Fig. 1 could be eliminated by use of equation (13). However, it was found that a piecewise linear fit was required for equation (11). It was therefore more convenient to transform equation (11) to

$$\alpha_{\text{eff}} = \alpha_0 + K'(\bar{\alpha} - \alpha_0) \tag{14}$$

where $K' = K - 1$.

With this format, the round tube data could be correlated through the following relations for α_{eff}:

$$\alpha_{\text{eff}} = \bar{\alpha} \qquad \bar{\alpha} \leqslant 0.642$$

$$\alpha_{\text{eff}} = 0.642 + 0.37(\bar{\alpha} - 0.642) \qquad 0.642 < \bar{\alpha} \leqslant 0.788$$

$$\alpha_{\text{eff}} = 0.696 + 0.2(\bar{\alpha} - 0.788) \qquad 0.788 < \bar{\alpha} \leqslant 0.81.$$

The results of using the foregoing relationships are as shown in the comparison of predicted and measured CHF values shown in Fig. 3. The data correlated are restricted to $0.64 \leqslant \alpha \leqslant 0.81$ but include

(a) The appropriate portion of the uniform axial heat flux data shown in Fig. 1.
(b) The applicable points from the non-uniform axial heat flux water data of Swenson *et al.* [15].
(c) The appropriate portion of the liquid N_2 data of Pappell *et al.* [16].
(d) The applicable portion of the Refrigerant 11 data of Leung [17].

It may be seen that reasonable agreement is obtained for each set of data. The effectiveness of the predictive procedure is quantitatively determined by using the parameter R (defined in equation 6). The values of the mean and standard deviation of R which are reported in Table 1 confirm the satisfactory nature of the procedure for both water Refrigerant 11. Although the value of $\mu(R)$ for nitrogen is 1.28, it must be noted that Weisman and Pei [4] found $\mu(R) = 1.3$ for the low void range. The slight underprediction of the Refrigerant 11 and water data is within the usual accuracy of DNB data. Although the underprediction could have been eliminated by revised constants, this leads to increased scatter.

Rod bundle DNB data were also found to behave in a manner similar to that seen for round tubes. The data chosen for examination were the high void points for water–steam system tests performed at Columbia University and described by Reddy and Fighetti [18]. These data included the three test series previously used by Weisman and Ying [8, 9] for their study of

Table 1. Statistical analysis of round-tube DNB data at high void fractions

Fluid	Void range	No. of pts.	$\mu(R)$	$\sigma(R)$
Water	0.642–0.81	52	0.95	0.11
R-11	0.64–0.8	14	0.952	0.06
Nitrogen	0.64–0.8	4	1.28	0.05

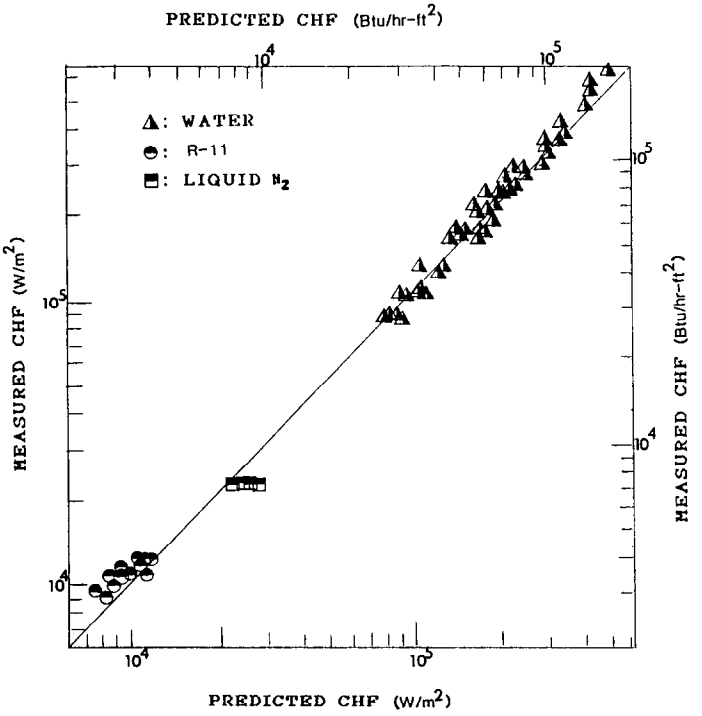

FIG. 3. Comparison of round tube DNB predictions and measurements at high voids.

rod bundle CHF at low voids. All of the data were for assemblies with simple support grids (*no* mixing vanes). Two test series were conducted with rods having a non-uniform axial heat flux distribution while in all the other series the rods had a uniform axial flux distribution.

In order to determine the local conditions along the hot channel, it is necessary to use a subchannel analysis code. Weisman and Ying [8, 9] made use of the results of the COBRA code [19] for this purpose. The predicted power was calculated using the reduction in the hot channel flow and enthalpy indicated by COBRA. The enthalpy was calculated by defining a mixing factor, $f_m(z)$, as

$$f_m(z) = \frac{\text{(Actual specific enthalpy rise per unit length in hot channel at) experimental conditions (from COBRA)}}{\text{(Specific enthalpy rise per unit length in closed channel with) same heat input as experiment}}. \quad (16)$$

The value of $f_m(z)$ was taken as being constant in a given channel at a given elevation at power levels close to the DNB flux. For length step i along the channel, the net heat input is

$$q_{\text{net},i} = q_i f_m(z_i). \quad (17)$$

The COBRA code input parameters were established so that the results obtained agreed with those previously obtained at low void fractions.

The available simple grid rod bundle data were predicted using an $x_{1_{\text{eff}}}$ determined through use of equation (14) (same procedure for high void, round tube data). Good results were obtained. For these predictions, $\mu(R) = 1.009$ and $\sigma(R) = 0.091$.

Since reactor designers would like to have correlation with as low a scatter as possible, an effort was made to see if a revised set of correlation for α_{eff} could reduce the value of $\sigma(R)$. A slightly improved set of predictions were obtained using the following:

$$\alpha_{\text{eff}} = \bar{\alpha} \quad \text{for } \bar{\alpha} < 0.62$$

$$\alpha_{\text{eff}} = 0.62 + 0.48(\bar{\alpha} - 0.62) \quad \text{for } 0.62 \leqslant \alpha < 0.72 \quad (18)$$

$$\alpha_{\text{eff}} = 0.668 + 0.37(\bar{\alpha} - 0.72) \quad \text{for } 0.72 < \alpha \leqslant 0.84.$$

The comparison of measurements and predictions for the 94 points examined is shown graphically in Fig. 4. The statistical evaluation of the comparison given in Table 2 shows that $\sigma(R)$ was reduced to 0.08.

To demonstrate that the approach taken for water data from rod bundles applied to other fluids, the rod bundle data of Cocilovo *et al.* [20] and Rudzinski [21] for Refrigerant 12 were examined. Both rod bundles used simple grid spacers. Although most of these data were at very high void fractions, 18 points in the desired void fraction range were found. The predictions obtained using equation (14) together with the Weisman–Pei prediction procedures are compared to experimental data in Fig. 5. Also shown for comparison are low void rod bundle (simple grid) data obtained by Motley *et al.* [22] for Refrigerant 11. It

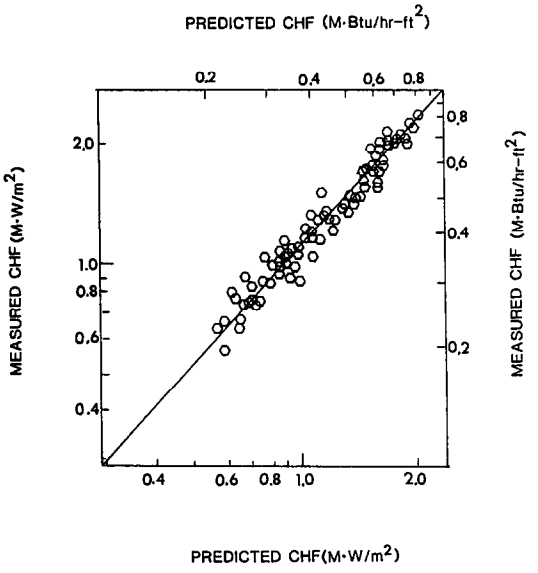

FIG. 4. Comparison of rod bundle DNB predictions and measurements at high voids.

may be seen that all of these data are adequately predicted. The statistical analysis showing the accuracy of the high void Refrigerant 12 data is shown in Table 2. The slight underprediction of the Refrigerant 11 and 12 data is believed to be within the usual accuracy of DNB data.

PREDICTION OF CHF LOCATION FOR NON-UNIFORM AXIAL FLUX

Although there were a few data points for non-uniform axial heat flux distributions among the round tube data, these were insufficient to provide a very meaningful test of the ability of the proposed

Table 2. Statistical analysis of rod bundle DNB data at high void fractions

Fluid	No. of pts	α_{eff} correlation	$\mu(R)$	$\sigma(R)$
Water	94	eqn (14)	1.009	0.091
Water	94	eqn (17)	0.99	0.08
R-12	18	eqn (14)	0.93	0.08

approach to predict CHF location at high voids. However, the non-uniform rod bundle data provide 21 points in the appropriate void fraction range. The predicted and measured CHF locations are compared in Fig. 6. The vertical lines through the points indicate the uncertainty in the measured CHF location (distance between CHF thermocouple and next thermocouple). It may be seen that moderately good agreement is obtained. It should be noted that predictions of CHF locations always tend to be considerably less precise than predictions of the heat flux itself.

EXTENSION OF THE THEORETICALLY BASED CHF CORRELATION TO LOW MASS FLOWS

Although previous work [7] indicated the Pei–Weisman correlation could be used down to mass flows of 1.8×10^6 kg/m² h (0.35×10^6 lb/m² ft²), there were essentially no data examined below 2.1×10^6 kg m² h (0.41×10^6 lb/h ft²). The data below this mass flux were at void fractions above the 0.6 limit previously imposed on the predictive procedure. At the 1.8×10^6 kg/m² h limit, DNB predictions were 5–10% below the measured values.

Since void fractions up to 0.80 can now be

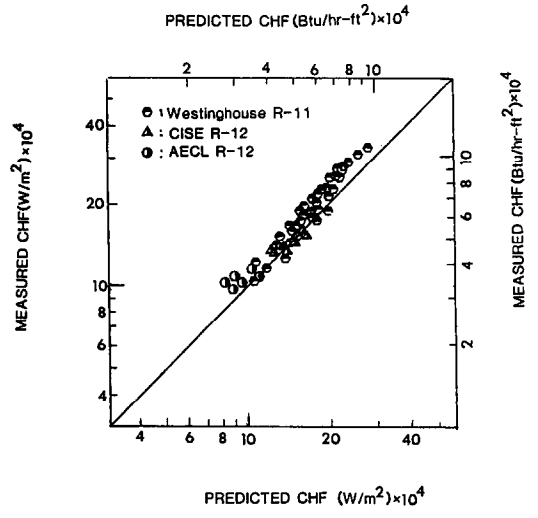

FIG. 5. Comparison of rod bundle DNB predictions and measurements for Refrigerant 11 and 12.

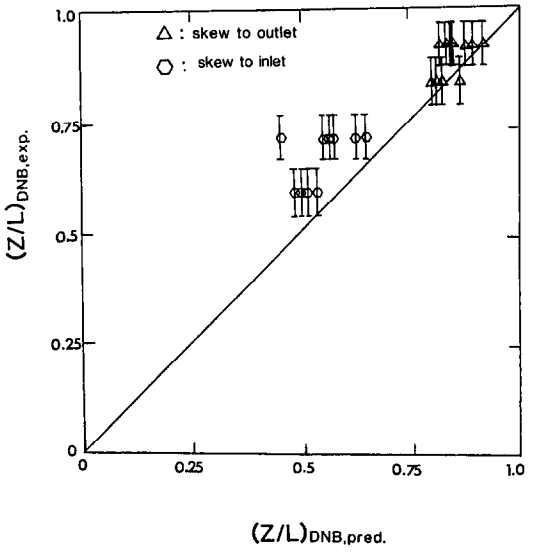

FIG. 6. Comparison of measured and predicted DNB locations along non-uniformly heated rod bundles.

considered, it was decided to re-examine the low mass flux data to see if the predictive procedure could be extended to lower velocities. The assumptions of the Pei–Weisman predictive procedure were first examined to see if they all remained applicable. This reanalysis noted that the Levy [23] model used for bubble size determination ignored buoyancy effects. Levy [23] originally assumed that the radius, r_b, of a bubble departing from a heated surface during flow boiling could be obtained from

$$C_B(g/g_c)(\rho_L-\rho_G)r_b^3+C_F(\tau_\omega/D_h)r_b^3-C_S r_b=0. \quad (19)$$

When this is rearranged to solve for r_b, one obtains

$$r_b=\left[C_S/C_F\left(\frac{\sigma D_h}{\tau_\omega}\right)\right]^{1/2} \div\left[1+(C_B/C_F)g/g_c\left(\frac{\rho_L-\rho_G}{\tau_\omega}\right)D_h\right]^{1/2} \quad (20)$$

or

$$r_b=C_1\left(\frac{\sigma D_h}{\tau_\omega}\right)^{1/2}(1+C_2(g/g_c)\left(\frac{\rho_L-\rho_G}{\tau_\omega}\right)D_h\Big]^{1/2}, \quad (21)$$

where $C_1=(C_S/C_F)^{1/2}$ and $C_2=C_B/C_F$.

C_B, C_F, C_S = buoyancy friction and surface force coefficients and other symbols used have their previous meaning.

Levy assumed that at high velocities only the frictional drag was significant and therefore set C_2 at zero. This formulation was that used by Weisman and Pei [4].

In the low velocity range, buoyant forces may no longer be negligible and the appropriate (non-zero) value of C_2 should be used. To determine the appropriate range for C_2, the early work of Fritz [24] on bubbles growing in a stagnant liquid was considered. Fritz [24] found

$$r_b=0.0104\beta_0[g_c\sigma/g(\rho_L-\rho_G)]^{1/2} \quad (22)$$

where β_0 = bubble contact angle in degrees.

When equation (19) is written for zero flow ($\tau_\omega=0$) and then solved for r_b

$$r_b=(C_S/C_B)^{1/2}[g_c\sigma/g(\rho_L-\rho_G)]^{1/2}. \quad (23)$$

Hence

$$0.014\beta_0=(C_S/C_B)^{1/2}. \quad (24)$$

Since Levy [23] concluded $C_1=(C_S/C_F)^{1/2}=0.015$, we have

$$C_2=C_B/C_F=(C_S/C_F)\cdot(C_B/C_S)=\frac{(0.015)^2}{(0.0104\beta_0)^2} \quad (25)$$

or $C_2=2.081/\beta_0^2$.

While the value of β_0 which should be used under the high pressure flow boiling situation of interest is not certain, we can use equation (25) to estimate the possible range for C_2. It is highly unlikely that $\beta_0<2^0$. If this is so, then the maximum value of C_2 is 0.5. Thus C_2 should be between 0 (Levy's assumption) and 0.5.

Various values of C_2 were examined. The value chosen was that which minimized the scatter of the low velocity round-tube water DNB data available from Thompson and Macbeth [10] on a plot of R vs liquid velocity. The best results were obtained using $C_2=0.1$. The values of R obtained with the value of C_2 are shown in Fig. 7. It will be noted that there is now an acceptable scatter in the water data but that as the inlet velocity is decreased below 1.4 m/sec there is an increasing deviation of R from 1.0.

Also shown in Fig. 7 are the low velocity liquid helium data of Katto and Yokoya [25]. Although the

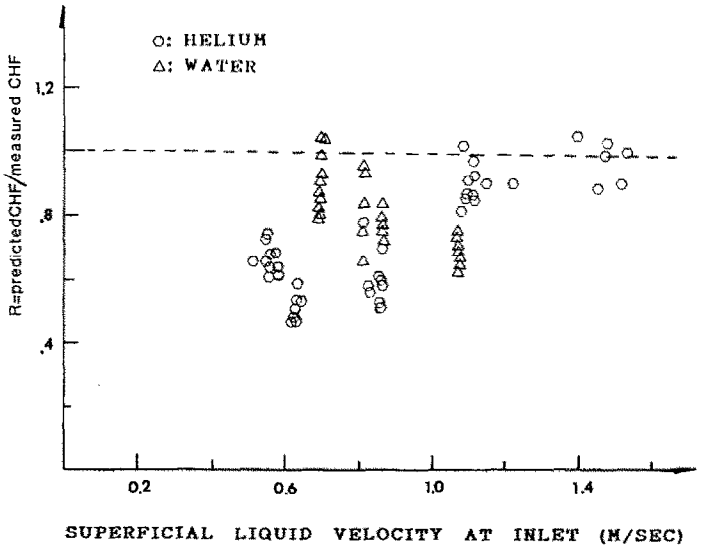

FIG. 7. Effect of superficial liquid inlet velocity on DNB predictions before revising turbulent intensity.

mass velocities at which the helium data were obtained are far below the mass velocities of the water data, the unusually low specific gravity of liquid helium leads to superficial liquid velocities, V_{SL}, in the same range as the water data. Although these data exhibit significant scatter, the predictions obtained are in the correct range. This is remarkable since the actual critical heat fluxes are three orders of magnitude below those for water.

It was postulated that the data at low velocities showed higher heat fluxes than predicted because buoyancy effects were more important at low flows. One would then expect that the two-phase multiplier on the turbulent intensity would increase as the flow rate decreases. In the expression for the turbulent intensity [equation (3)] used by Weisman and Pei [4], the two-phase multiplier is $[1+a(\rho_L-\rho_G)/\rho_G]$. Although Weisman and Pei [4] found "a" to be constant for $3.6\times10^6 < G < 9.7\times10^6\,\text{kg/m}^2\,\text{h}$, they found it necessary to have "a" decrease with increasing G. Values of "a" which increases as the flow decreased at low velocities are consistent with the overall trend.

Although the water data could be readily correlated by making "a" vary with the total mass velocity, G, it was decided to use V_{SL} as the correlating parameter so that the helium data could also be included. The best results were obtained with

$$a = 0.87(1.36-V_{SL})+0.135;$$
$$0.5 < V_{SL} < 1.36\,\text{m/sec}. \quad (26)$$

To be consistent, we have at higher velocities

$$a = 0.135;$$
$$G < 9.7\times10^6\,\text{kg m}^2\,\text{h},\ V_{SL} > 1.36\,\text{m/sec}. \quad (27)$$

Table 3. Statistical evaluation of predictions at low flow ($0.5 < V_{SL} < 1.36$ m/sec)

Fluid	No. of data pts	$\mu(R)$	$\sigma(R)$
Water	32	0.96	0.072
Helium	30	0.87	0.13

The results of the revised predictions are shown in Fig. 8. In making these predictions, equation (13) was used. The relationship between x and α followed the recommendation of Weisman and Ying [7, 8] as described previously. It may be seen in Fig. 8 that the water data are well correlated and a moderately good correlation is obtained for the helium data. Note that the ratio $[(\rho_L-\rho_G)/\rho_G]$ is substantially different for the helium and water data. The fact that reasonable agreement is obtained between the two sets of data would seem to substantiate the density ratio correction used. Statistical analyses of the results are presented in Table 3.

It was considered possible that a dimensionless group, based on liquid velocity (such as the square root of the Froude number) might provide a preferable correlating parameter for "a". However, when the $(Fr)^{1/2}$ is used to replace V_{SL} the helium predictions were substantially above the water data at the lower flow rates. It was therefore concluded that V_{SL} was the better correlating parameter.

CONCLUSION

By making appropriate allowance for the fact that the radial void profile at high void fractions is not uniform, it has been possible to extend the Weisman–

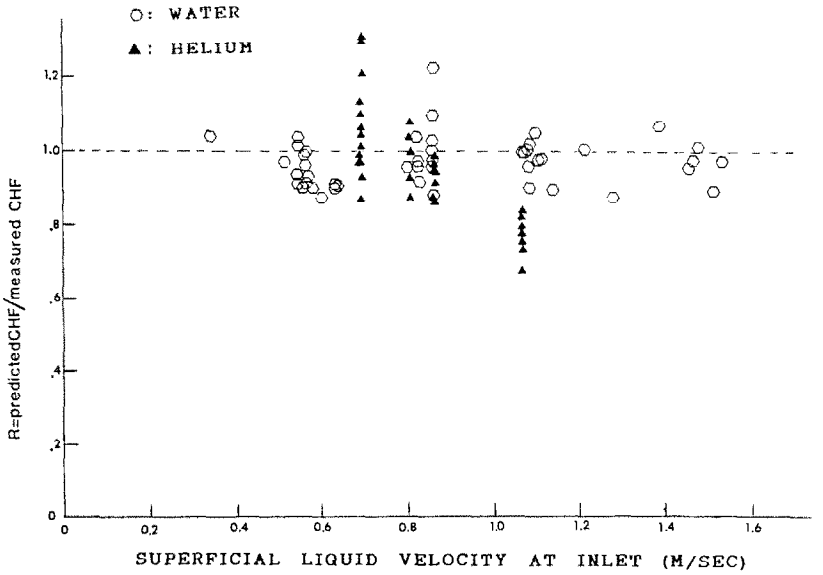

FIG. 8. Effect of superficial liquid inlet velocity on final DNB predictions in round tubes.

Pei theoretically based DNB prediction from void fractions in the neighborhood of 0.6 to void fractions of 0.8. This results in a significant increase in the maximum allowable quality. At 35 bar the maximum allowable quality for the steam–water system is increased from 3% to 8% while at 140 bar it increases from 18% to 35%.

Behavior in both round tubes and rod bundles is consistent. The same relationships between the average void fraction, $\bar{\alpha}$, and α_{eff}, the void fraction just outside the bubbly layer, could be used for the two geometries. However, somewhat reduced scatter of the rod bundle data were obtained with a slightly revised relationship.

It is believed that the new restriction of $\alpha \leqslant 0.8$ is close to the upper limit at which the DNB mechanism applies. At higher void fractions, the critical heat flux may be expected to be controlled by the dry-out phenomenon and the present approach would be inapplicable.

The ability to predict behavior at higher void fractions allowed examination of the behavior at low mass fluxes where void fractions are generally high. Successful prediction of these data were obtained by modification of the turbulent intensity two-phase multiplier.

Acknowledgement—The authors wish to acknowledge the financial support of the Nuclear Fuel Division of the Westinghouse Electric Corp. which made this work possible.

REFERENCES

1. N. Zuber, On stability of boiling heat transfer, *Trans. ASME* **80,** 711 (1958).
2. R. G. Vanderwater, An analysis of burnout in two-phase liquid vapor flow, Ph.D. Dissertation, University of Minnesota, Minneapolis, MN (1957).
3. H. S. Isbin, R. Vandewater, H. Fauske and S. Singh, A model for correlating two-phase, steam–water, burnout heat fluxes, *Trans. ASME J. Heat Transfer* **83,** 149 (1961).
4. J. Weisman and B. S. Pei, Prediction of critical heat flux in flow boiling at low qualities, *Int. J. Heat Mass Transfer* **26,** 1463 (1983).
5. L. S. Tong, H. B. Currin, P. S. Larsen and D. G. Smith, Influence of axially non-uniform heat flux on DNB, *A.I.Ch.E. Symp. Ser.* **64,** 35 (1965).
6. L. M. Jiji and J. A. Clark, Bubble boundary layer and temperature profiles for forced convection boiling in channel flow, *Trans. ASME (C), J. Heat Transfer* **86,** 50–61 (1964).
7. J. Weisman and S. H. Ying, Theoretically based CHF predictions at low qualities and intermediate flows, *Trans. ANS* **45,** 832 (1983).
8. J. Weisman and S. H. Ying, A theoretically based DNB prediction for rod bundles, *Trans. ANS* **47,** 571 (1984).
9. J. Weisman and S. H. Ying, A theoretically based DNB prediction for rob bundles at PWR conditions, *Nucl. Engng Design* **85,** 239 (1985).
10. B. Thompson and R. Macbeth, Boiling water heat transfer burnout in uniformly heated round tubes—a compilation of world data with accurate correlations, UKAE Rep. No. HEEW-R356 (1964).
11. A. Serizawa, Fluid dynamics characteristics of two-phase flow, Ph.D. Thesis, Kyoto University, Japan (1974).
12. D. A. Drew and R. T. Lahey, Phase distribution in turbulent low quality two-phase flow in a circular pipe, *J. Fluid Mech.* **117,** 91 (1982).
13. R. Van der Welle, Void fraction, bubble velocity and bubbler size in two-phase flow, *Int. J. Multiphase Flow* **11,** 161 (1985).
14. K. W. McQuillan and P. B. Whalley, Flow patterns in vertical two-phase flow, *Int. J. Multiphase Flow* **11,** 161 (1985).
15. H. S. Swenson, J. R. Carver and C. R. Kakarala, The influence of axial heat flux distribution on the departure from nucleate boiling in water cooled tubes, ASME Paper 62-WA-2978 (1962).
16. S. S. Pappell, R. J. Simoneau and D. D. Brown, Buoyancy effects on critical heat flux of forced convective boiling in vertical flow, NASA Report TND-3672, Washington, DC (1966).
17. J. C. Leung, Transient critical heat flux and blowdown heat transfer studies, Nuclear Regulatory Comm. Rep. NUREG CR-1559 (ANL-80-53) (1980).
18. D. G. Reddy and C. F. Fighetti, Parametric study of CHF data, Vol. 3, Critical heat flux data, EPRI Rep. NP-2609. Electric Power Research Inst., Palo Alto, CA (1983).
19. D. S. Rowe, COBRA IIIC; a digital computer program for steady state transient thermal analysis of rod bundle nuclear fuel elements, Rep. BNWL-1965, Battelle Northwest Laboratory, Richland, WA (1973).
20. M. Cocilovo, M. Cumo and G. Palazzi, On DNB location with axially disuniform heat flux profiles, an experimental contribution, Rep. CNEN-RT/ING(79)21 C.I.S.E., Rome, Italy (1979).
21. K. F. Rudzinski, Eighteen element Freon CHF experiment using grid spaces, Rep. CRNL-1344 Atomic Energy of Canada Ltd, Chalk River, Canada (1976).
22. F. E. Motley, F. F. Cadek, J. O. Cermak, L. Stoney, S. W. Gouse, F. Paul and J. C. Purcupile, CHF data from Freon 11 for scaling CHF in water, *Int. Symps. Two-Phase Systems*, Aug.–Sept. 1981, The Technion, Haifa, Israel (1981).
23. S. Levy, Forced convection subcooled boiling–prediction of vapor volumetric fraction, Rep. GEAP-5157 General Electric Co. (1966).
24. W. Fritz, Maximum value of vapor bubbles, *Physik Zeitschr.* **36,** 379–384 (1935).
25. Y. Katto and S. Yokoya, Critical heat flux of liquid helium in forced convective boiling, *Int. J. Multiphase Flow* **10,** 401 (1984).

PREDICTION DU FLUX DE CHALEUR CRITIQUE DANS L'EBULLITION AVEC ECOULEMENT POUR DES QUALITES INTERMEDIAIRES

Résumé—Pour un profil de vide non uniforme on trouve que la procédure de calcul de flux critique théorique précédemment développée peut être étendue jusqu'à des fractions de vide de 0,8. L'approche générale est valable pour des tubes à section circulaire et des grappes de tubes. Les données expérimentales avec l'eau et autres fluides sont prévues par cette approche. La capacité de prédire les flux thermiques critiques aux qualités élevées fournit la possibilité d'extension au cas des faibles débits-masse pour lesquels les fractions de vide sont généralement grandes.

BERECHNUNG DER KRITISCHEN WÄRMESTROMDICHTE BEIM STRÖMUNGSSIEDEN BEI MITTLEREN DAMPFGEHALTEN

Zusammenfassung—Es zeigt sich, daß die bereits früher theoretisch entwickelte Gleichung zur Berechnung der kritischen Wärmestromdichte (CHF) bis zu Dampfgehalten von 0,8 erweitert werden kann, wenn man ein nichtgleichförmiges Profil des Dampfgehaltes zuläßt. Die allgemeine Näherung gilt sowohl für runde Rohre als auch für Rohrbündel mit einfachen Abstandshaltern. Die Beziehung kann für Wasser und andere Stoffe angewandt werden. Die Möglichkeit, die kritische Wärmestromdichte bei höheren Dampfgehalten vorauszuberechnen, erlaubt es, das Berechnungsverfahren auf geringe Massenstromdichten zu erweitern, wo die Dampfgehalte bei CHF gewöhnlich hoch sind.

РАСЧЕТ КРИТИЧЕСКОГО ТЕПЛОВОГО ПОТОКА В УСЛОВИЯХ ТЕЧЕНИЯ ПРИ КИПЕНИИ С ПРОМЕЖУТОЧНЫМИ СВОЙСТВАМИ

Аннотация—С учетом неоднородного профиля паросодержания найдено, что ранее разработанная теоретически обоснованная методика расчета критического теплового потока может быть применима при паросодержаниях вплоть до 0,8. Общий подход имеет силу как для круглых труб, так и для пучков стержней с простыми решетками. С помощью данного метода расчета получены результаты для воды и других жидкостей. Возможность рассчитывать критический тепловой поток более качественно позволила распространить процедуру расчета на более низкие скорости массового потока, при которых паросодержание при КТП обычно является высоким.